Macromolecular Rapid Communication
www.mrc-journal.de

Self-Assembly of Rod-Coil Block Copolymers on Carbon Nanotubes: A Route toward Diverse Surface Nanostructures

Yang Han, Chunhua Cai, Jiaping Lin,* Shuting Gong, Wenheng Xu, and Rui Hu*

In this work, it is reported that poly(γ-benzyl-L-glutamate)-*block*-poly(ethylene glycol) (PBLG-*b*-PEG) rod-coil block copolymers (BCPs) can disperse carbon nanotubes (CNTs) in solution and form various surface nanostructures on the CNTs via solution self-assembly. In an organic solvent that dissolves the BCPs, the PBLG rod blocks adsorb on CNT surfaces, and the BCPs form conformal coatings. Then, by the introduction of water, a selective solvent for PEG blocks, the BCPs in the coatings further self-assemble into diverse surface nanostructures, such as helices (left-handed or right-handed), gyros, spheres, and rings. The morphology of the surface nanostructure can be tailored by initial organic solvent composition, preparation temperature, feeding ratio of BCPs to CNTs, degree of polymerization of PBLG blocks, and diameter of the CNTs.

1. Introduction

Carbon nanotubes (CNTs) have attracted much attention in the fields of nanotechnology and materials science over the past decade.[1] Much effort has been exerted to disperse CNTs by small molecules and polymers in various media, and both physical and chemical approaches have been established.[2] Physically adsorbing polymers is an effective way to disperse CNTs without damaging their inherent properties. Polymer/CNT composites have found applications in broad fields ranging from reinforcing additives for polymer materials to biosensors and delivery vehicles.[3] Considering that the surface nanostructure of a material is an important factor that influences its properties,[4] in addition to the issue of dispersion, the surface nanostructures of polymer/CNT composites could be an emerging research topic.[5] However, apart from polymer crystallization,[6] few feasible methods are currently available to produce ordered surface nanostructures on CNTs.

Block copolymers (BCPs) can self-assemble into a variety of morphologies in solution and have found applications in various fields.[7] Recently, BCPs are particularly attractive as efficient dispersants for CNTs in solution, with one block attaching to the CNT, and the other extending into solvent.[8] However, conformal coating of BCPs on CNTs is achieved in most cases. One reason for the failure to prepare diverse surface nanostructures could be the use of coil-coil BCPs in these studies. Compared with coil-coil BCPs, rod-coil BCPs possess some unique self-assembly behaviors. For example, they tend to form ordered morphologies owing to the ordered packing tendency of the rigid blocks.[9] In our recent work, we found that poly(γ-benzyl-L-glutamate)-*block*-poly(ethylene glycol) (PBLG-*b*-PEG) rod-coil BCPs can self-assemble in water into various ordered nanostructures.[10] Therefore, we envisage that rod-coil BCPs may be ideal candidates for constructing ordered surface nanostructures on CNTs via solution self-assembly.

Herein, we demonstrate that PBLG-*b*-PEG rod-coil BCPs can serve as effective dispersants for CNTs in solution and that various surface nanostructures can be formed by BCPs on the CNTs. PBLG-*b*-PEG is a typical rod-coil block copolymer in which the PBLG is a synthetic polypeptide, the backbone of which adopts an α-helix conformation acting as a rigid rod, and PEG is a typical flexible polymer. As shown in **Scheme 1**, the preparation process for the PBLG-*b*-PEG/CNT dispersions in different solutions is as follows. First, in organic solvents that dissolve the BCPs and with the aid of sonication, CNTs are debundled into single tubes, and the PBLG-*b*-PEG BCPs adsorb onto the CNTs to act as a stabilizer. In the second step, by introducing water, a selective solvent for PEG blocks, the BCPs adsorbed on the CNTs further self-assemble into various ordered surface nanostructures, for example, helices.

2. Results and Discussion

We first investigated the dispersing properties of $PBLG_{119}$-*b*-PEG_{112} BCPs (the subscripts denote the degree of polymerization, DP, for each block) for CNTs in organic solvents. For convenience, the $PBLG_{119}$-*b*-PEG_{112} BCPs are abbreviated as BCP1 in the following content. *N*,*N*′-dimethylformamide (DMF, a high-polar solvent) and 1,4-dioxane (dioxane, a low-polar solvent) were used as typical solvents. **Figure 1** shows the results obtained using DMF as solvent, and the results from the dioxane system are presented in the Supporting Information. As shown in Figure 1a, digital photographs reveal that pristine CNTs were homogeneously suspended in DMF by sonication

Y. Han, Dr. C. Cai, Prof. J. Lin, S. Gong, W. Xu, R. Hu
Shanghai Key Laboratory of Advanced Polymeric Materials
State Key Laboratory of Bioreactor Engineering
Key Laboratory for Ultrafine Materials of Ministry of Education
School of Materials Science and Engineering
East China University of Science and Technology
Shanghai 200237, China
E-mail: caichunhua@ecust.edu.cn; jlin@ecust.edu.cn

The ORCID identification number(s) for the author(s) of this article can be found under https://doi.org/10.1002/marc.201800080.

DOI: 10.1002/marc.201800080

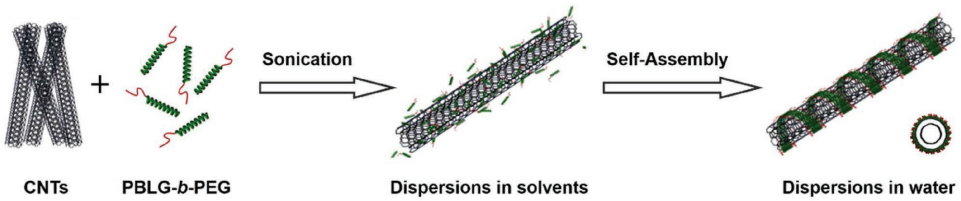

Scheme 1. Schematic illustration of the dispersion of CNTs by PBLG-*b*-PEG rod-coil BCPs in organic solvents and water.

(sample A), but they rapidly precipitated (sample B). In contrast, the BCP1/CNT mixtures (the feeding weight ratio, WR, of BCPs to CNTs is 2) showed high stability, and no apparent sediment was observed after standing for two months (sample C).

The optimal WR for dispersion was determined by recording UV–vis–IR absorption intensities.[3a,11] As shown in Figure 1b, the absorption intensity first increased markedly with the WR when the WR < 2 and then increased slightly with further increasing WR, which suggests the optimal WR is ≈2. Compared with other surfactants and polymer dispersants,[12] the rod-coil BCPs used in this work also possess excellent dispersing efficiency for CNTs while requiring a lower dispersant WR with the CNTs. In the following, unless otherwise noted, all samples were prepared with a WR = 2.

The structures of the BCP1/CNT dispersions were then examined by scanning electron microscopy (SEM) and transmission electron microscopy (TEM). As shown in Figure 1c, separated fibres with smooth surfaces were observed. The TEM image clearly reveals the core–shell structure of the fibres (Figure 1d). A single CNT (indicated by the blue arrows, with a diameter of ≈70 nm) was covered by a thin polymer coating (indicated by the red arrows, with a thickness of 30–40 nm).

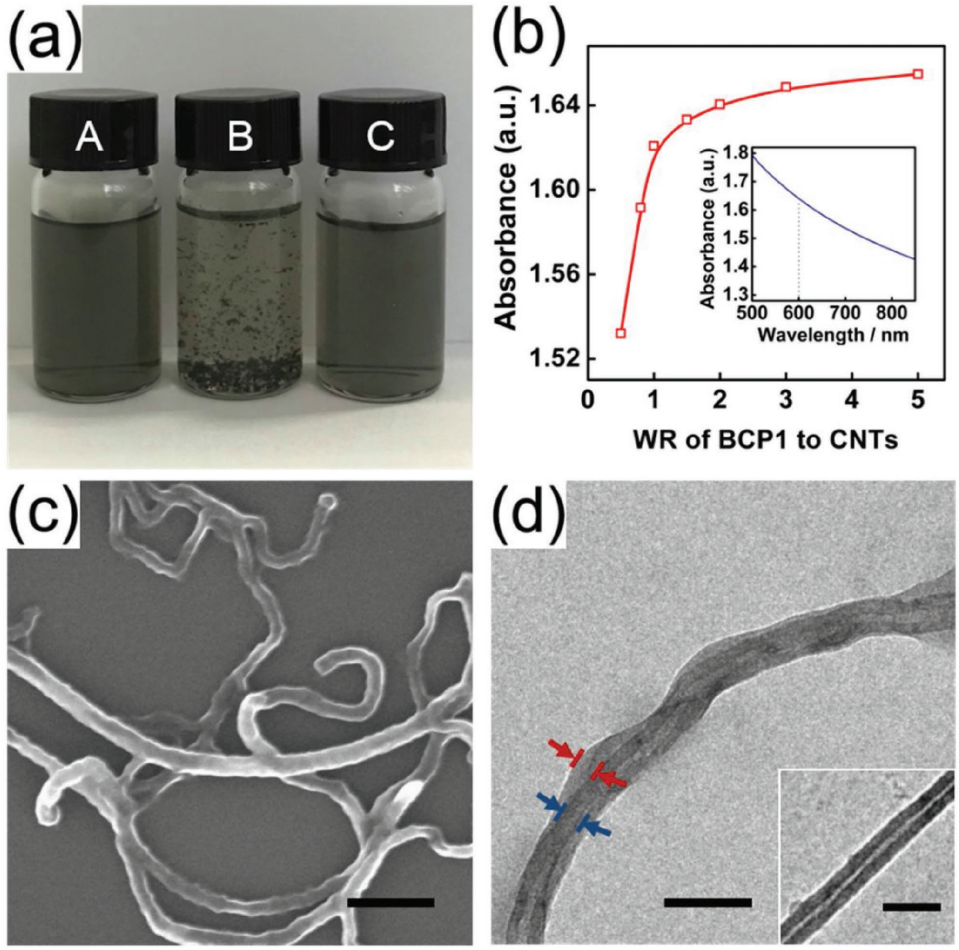

Figure 1. a) Digital photographs of pristine CNTs (A: immediately after sonication, and B: stored for 1 h) and BCP1/CNT dispersions (C: stored for two months) in DMF. b) UV–vis–IR absorption (recorded at a wavelength of 600 nm) of the BCP1/CNT dispersions in DMF as a function of the feeding WR of BCP1 to CNTs. The inset shows the absorption spectrum of the BCP1/CNT dispersion at WR = 2. c) SEM and d) TEM images of the BCP1/CNT dispersions in DMF. The inset shows TEM image of pristine CNT. Scale bars: c) 500 nm, d) 200 nm, and inset: 100 nm.

The inset in Figure 1d shows TEM image of pristine CNT. Similar properties and structures for the BCP1/CNT dispersions with dioxane as the solvent were observed. Details regarding the dispersing properties of BCP1 for CNTs are available in the Supporting Information (Figures S2 and S3, Supporting Information).

In organic solvents, the attractions (π–π interactions) between the phenyl groups of PBLG blocks and CNTs are inferred to play a key role in the dispersion of CNTs.[8a] To verify this assumption, control experiments using PBLG and PEG homopolymers to disperse pristine CNTs were performed. It was found that the PBLG homopolymers well stabilized CNTs in both DMF and dioxane. However, for the PEG/CNT mixtures, abundant precipitates were observed in a short time upon standing. These results proved that the formation of the PBLG-*b*-PEG/CNT dispersions in organic solvents is mainly due to the attractions between the PBLG blocks and CNTs, while the PEG blocks barely prevent the precipitation of the CNTs; however, PEG blocks could also enhance the dispersibility of the dispersions. Details are presented in Section S5 (Supporting Information).

To prepare BCP1/CNT dispersions in aqueous solutions, water was added to the BCP1/CNT dispersions in DMF or dioxane. Upon adding water, the solubility of the hydrophobic PBLG blocks decreased, which drove the BCPs to adsorb more tightly on the CNTs due to the hydrophobic–hydrophobic attractions between the PBLG blocks and CNTs. And under the hydrophobic/hydrophilic balance of the BCPs, they self-assembled into various surface nanostructures.[7] In the surface nanostructures, the hydrophobic PBLG blocks attached to the CNT surfaces, and the hydrophilic PEG blocks spread out into the water. Through dialysis against water, aqueous solutions of BCP1/CNT dispersions were obtained. The influences of the initial solvent composition and preparation temperature on the morphology of the surface nanostructures were first investigated (**Figure 2**).

Figure 2a–c shows the influence of the initial solvent composition on the morphology of the surface nanostructures. When DMF was used as the initial solvent, as shown in Figure 2a, individual plain fibres were observed. The diameters of these fibres (130–150 nm) were significantly larger than those of the pristine CNTs (60–80 nm), indicating that BCP1 adsorbed onto the CNTs. With dioxane as the initial solvent, the BCPs formed gyro-like nanostructures on the CNTs (Figure 2b). Interestingly, a distinct morphology (a helical nanostructure) was obtained using DMF/dioxane (1/1 in volume) as the initial solvent (Figure 2c). The solubilities of the PBLG-*b*-PEG BCPs in DMF, dioxane, and DMF/dioxane (1/1 in volume) differed considerably, which could be the reason for the formation of distinct surface nanostructures.

Figure 2d–f shows the morphologies of the samples prepared at a higher temperature (60 °C). When prepared with DMF or dioxane as the initial solvent, increasing the preparation temperature exerted no considerable effect on the surface nanostructures (Figure 2d,e). When using a DMF/dioxane mixture (1/1 in volume) as the initial solvent, the helical nanostructures formed at a higher temperature possessed more evident and regular helical features (Figure 2f). These helical nanostructures were further characterized by TEM and atomic force microscopy (AFM). As shown in Figure 2g, the TEM image clearly shows a core–shell structure, that is, block copolymers forming helical nanostructures around the CNTs. The 3D AFM image reveals these helical nanostructures possessed a right-handed chirality and a uniform pitch of ≈100 nm (Figure 2h), which is in good agreement with the SEM and TEM observations.

Note that the BCP1/CNT helical surface nanostructures shown in Figure 2f–h exclusively possessed a right-handed chirality. As widely reported in the literature, the chirality of chiral aggregates can be changed using stereoisomers (including polymers) bearing opposite chirality.[13] In this work, as shown in Figure 2i, left-handed helical surface nanostructures on CNTs were successfully fabricated by $PBDG_{114}$-*b*-PEG_{112} (PBDG: poly(γ-benzyl-D-glutamate)) under the corresponding experimental conditions (PBDG possesses a helical backbone with opposite chirality to that of PBLG[10a,b]).

Self-assembly of BCPs on CNTs into helices is rarely observed, which is an interesting finding of this work. In the past decade, there are several reports regarding helical wrapping of single polymers around CNTs.[14] However, because of the size limitation of polymer chains, those helical surface nanostructures are not as obvious as those reported in our present work. The helical wrapping of single polymers is found to enhance properties of or give additional functionality to composites. We expect that the BCP/CNT composites possessing higher dimensions and more obvious helical surface nanostructures will display performance superior to that of polymer-wrapped CNT composites.

As previously stated, when prepared at 60 °C with DMF/dioxane (1/1 in volume) as the initial solvent, the morphology of surface nanostructures is more regular and uniform. Under this condition, we investigated the influence of various factors, including the feeding WR of the BCPs to CNTs, the PBLG block length, and the CNT diameter, on the morphology of surface nanostructures. These results are presented in **Figure 3**. Stable CNT dispersions are obtained as the WR reaches 0.5, as the dispersions retain high stability after storage for more than two months (Figure S5, Supporting Information). The morphology of surface nanostructures markedly varied with the WR. At a lower WR (<1), no regular pattern was prepared. As shown in Figure 3a, at a WR = 0.5, BCPs formed rough coatings on the CNTs. Increasing the WR induces the formation of helical nanostructures. For example, well-defined helical nanostructures were observed at a WR = 1.5 (Figure S6c, Supporting Information) or 2 (Figure 2f). As the WR exceeded 3, small aggregates appeared in solution accompanied by helical nanostructured dispersions (see Figure 3b, WR = 5). These small aggregates should be micelles self-assembled by the BCPs themselves, which consist of PBLG core and PEG corona. And portion of the micelles increased with the WR. The surface morphology transition from a rough surface to helical nanostructure could be induced by a variation of the aggregation number (N_{agg}) of the BCP in the surface nanostructures. N_{agg} is a key factor influencing the structure and morphology of BCP self-assemblies.[15] The above results indicate that to prepare stable BCP1/CNT dispersions with no free accompanying micelles, a WR of ≈2 is required, which coincides well with the conclusion that the optimal WR is 2 for dispersing CNTs in organic solvents.

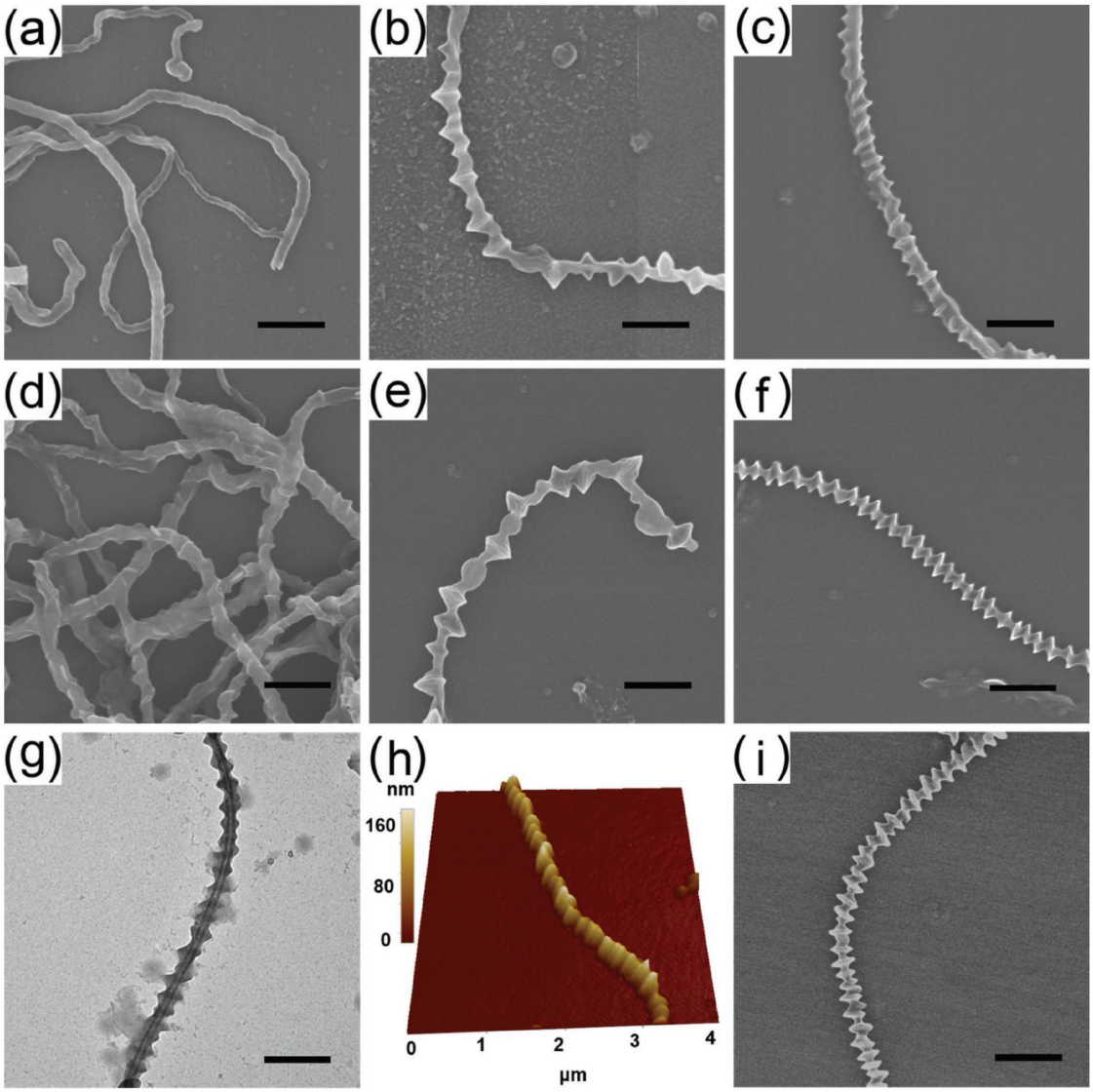

Figure 2. SEM images of BCP1/CNT dispersions in water prepared at 30 and 60 °C with various initial solvents: a) DMF, 30 °C; b) dioxane, 30 °C; c) DMF/dioxane (1/1 in volume), 30 °C; d) DMF, 60 °C; e) dioxane, 60 °C; and f) DMF/dioxane (1/1 in volume), 60 °C. g) TEM and h) AFM images of the sample shown in panel (f). i) SEM image of the PBDG-*b*-PEG/CNT dispersion prepared at 60 °C with DMF/dioxane (1/1 in volume) as the initial solvent. The WR = 2 for all samples. Scale bars: 500 nm.

The PBLG block length (degree of polymerization, DP) and the CNT diameter also markedly affected the morphology of surface nanostructures. A plain fibre-to-helix-to-sphere morphology transition was observed with increasing DP of the PBLG blocks. From well-established self-assembly principles,[7] the morphology of the surface nanostructures is a result of balance between attraction (PBLG–PBLG pairs) and repulsion (PEG–PEG pairs) interactions of BCPs. Since PEG block length is fixed, the repulsion between PEG–PEG blocks remain unchanged. The main reason for such morphology transition is induced by variation of the PBLG–PBLG attractions. When the DP of PBLG blocks is relatively small ($PBLG_{21}$-*b*-PEG_{112}, BCP2), the attraction between PBLG blocks is weak, therefore PBLG blocks pack randomly on the CNTs and a plain surface is obtained (Figure S8, Supporting Information). With increasing the DP of PBLG blocks ($PBLG_{119}$-*b*-PEG_{112}, BCP1), the attraction between PBLG blocks is enhanced, which induces PBLG blocks pack orderly into helix nanostructures (Figure 2f). When the DP of the PBLG blocks is relatively large ($PBLG_{210}$-*b*-PEG_{112}, BCP3), the attraction between PBLG blocks is strong, which restricts the morphology evolution in self-assembly process,[16] resultantly, discrete spheres on the surface of CNTs are formed (Figure 3c). Shown in Figure 3d is morphology of BCP1/CNT dispersion prepared using CNTs with a large diameter (OD = 140–160 nm). As can be seen, BCP1 formed ring-like structures wrapped around the CNTs. This morphology transition was inferred to be related to variation of surface curvature of the CNTs (the surface curvature of the CNT decreases with increasing the diameter).[17]

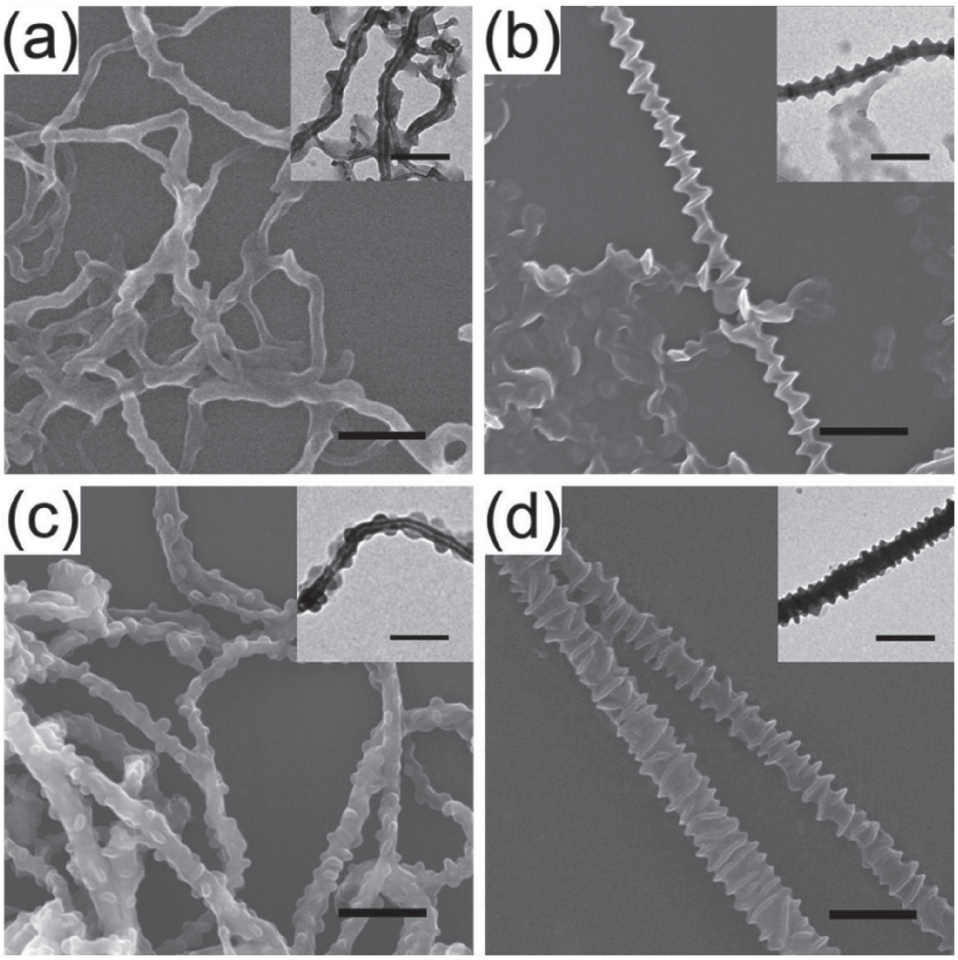

Figure 3. SEM images of various BCP/CNT dispersions in water: a) BCP1/CNT, WR = 0.5; b) BCP1/CNT, WR = 5; c) BCP3/CNT, WR = 2; and d) BCP1/CNT (CNT with a larger diameter), WR = 2. All samples were prepared at 60 °C with DMF/dioxane (1/1 in volume) as the initial solvent. Scale bars: 500 nm, and insets: 200 nm.

Additionally, for some practical applications, water dispersions of nanomaterials must be lyophilized to facilitate their storage and application. It was found that the BCP/CNT nanocomposites preserved their surface nanostructures after lyophilization, and these lyophilized samples were re-dispersible in water. With the aid of sonication and gentle magnetic stirring, single-fibre-level dispersions were obtained. Details regarding the storage stability and re-dispersibility results are presented in Section S10 (Supporting Information).

Finally, the noncovalent modification of CNTs by PBLG-*b*-PEG BCPs was confirmed by Raman spectroscopy. As shown in **Figure 4**, both pristine CNTs and BCP1/CNT dispersions exhibited D (defect) bands at 1312 cm^{-1} and G (graphene) bands at 1600 cm^{-1}. The intensity ratio of the D band to the G band (I_D/I_G) is sensitive to the defect concentration in CNTs, which is commonly used to identify the physical or chemical modification of CNTs.[8a,18] No clear change in I_D/I_G was observed (2.70 for the pristine CNTs vs 2.67 for the BCP1/CNT dispersions), suggesting that no chemical reaction occurred and that the CNTs were physically stabilized by the PBLG-*b*-PEG block copolymers.

3. Conclusions

In summary, we demonstrated a facile method, that is, the self-assembly of rod-coil block copolymers on CNTs, to construct various surface nanostructures, including helices, gyros, spheres, and rings. The self-assembly of PBLG-*b*-PEG rod-coil block copolymers was triggered by adding water to the BCP/CNT dispersions in organic solvents. The morphology of the surface nanostructures could be tailored by various factors, such as the initial organic solvent, the preparation temperature, the feeding ratio of the block copolymer to CNTs, the DP of the PBLG blocks, and the CNT diameter. Since both PBLG and PEG blocks possess biocompatibility, it can be expected that the formation of PBLG-*b*-PEG surface nanostructures on CNTs could not only enhance their biocompatibility but also provide additional functionality endowed by the surface nanostructures. These surface nanostructured polymer/CNT composites could find potential applications in biomedical areas, such as delivery vehicles for drugs and tissue regeneration scaffolds for nerves and bones.

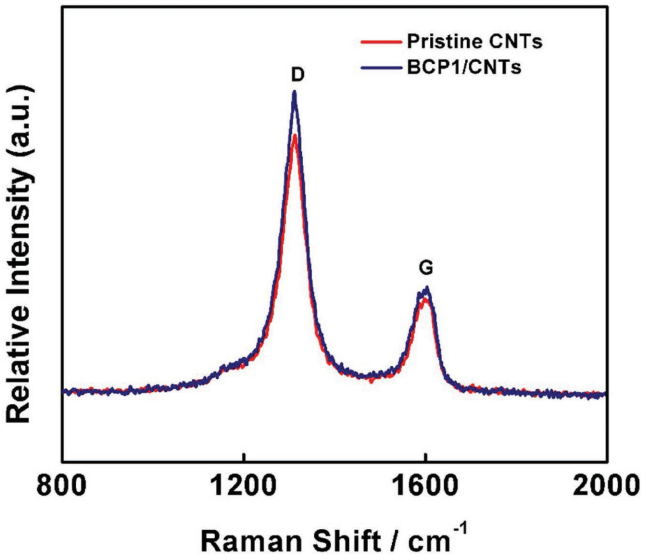

Figure 4. Raman spectra of pristine CNTs and BCP1/CNT dispersions in water (excitation wavelength: 785 nm). The BCP1/CNT samples were prepared at 60 °C with DMF/dioxane (1/1 in volume) as the initial solvent (the morphology of this sample is shown in Figure 2f–h).

Supporting Information

Supporting Information is available from the Wiley Online Library or from the author.

Acknowledgements

This work was supported by the National Natural Science Foundation of China (51573049 and 21474029). Support from the Project of Shanghai Municipality (15QA1401400) and Fundamental Research Funds for the Central Universities (222201717021) is also appreciated.

Conflict of Interest

The authors declare no conflict of interest.

Keywords

aqueous dispersion, carbon nanotube, rod-coil block copolymer, self-assembly, surface nanostructure

Received: January 29, 2018
Revised: March 2, 2018
Published online: April 14, 2018

[1] a) M. F. L. De Volder, S. H. Tawfick, R. H. Baughman, A. J. Hart, *Science* **2013**, *339*, 535; b) D. Tasis, N. Tagmatarchis, A. Bianco, M. Prato, *Chem. Rev.* **2006**, *106*, 1105; c) G. G. Kumar, S. Hashmi, C. Karthikeyan, A. GhavamiNejad, M. Vatankhah-Varnoosfaderani, F. J. Stadler, *Macromol. Rapid Commun.* **2014**, *35*, 1861.
[2] a) C.-W. Huang, M. G. Mohamed, C.-Y. Zhu, S.-W. Kuo, *Macromolecules* **2016**, *49*, 5374; b) X. Peng, S. S. Wong, *Adv. Mater.* **2009**, *21*, 625; c) D. Tuncel, *Nanoscale* **2011**, *3*, 3545; d) S. Y. An, S. Sun, J. K. Oh, *Macromol. Rapid Commun.* **2016**, *37*, 705.
[3] a) A. Ezzeddine, Z. Chen, K. S. Schanze, N. M. Khashab, *ACS Appl. Mater. Interfaces* **2015**, *7*, 12903; b) T. Gegenhuber, M. Krekhova, J. Schöbel, A. H. Gröschel, H. Schmalz, *ACS Macro Lett.* **2016**, *5*, 306; c) C. Li, S. Bolisetty, K. Chaitanya, J. Adamcik, R. Mezzenga, *Adv. Mater.* **2013**, *25*, 1010.
[4] a) J. Xue, Z. Guan, J. Lin, C. Cai, W. Zhang, X. Jiang, *Small* **2017**, *13*, 1604214; b) H. Assender, V. Bliznyuk, K. Profyrakis, *Science* **2002**, *297*, 973.
[5] a) J. Montenegro, C. Vázquez-Vázquez, A. Kalinin, K. E. Geckeler, J. R. Granja, *J. Am. Chem. Soc.* **2014**, *136*, 2484; b) Z. Tan, H. Abe, *ACS Macro Lett.* **2014**, *3*, 35; c) N. Yu, X. Zheng, Q. Xu, L. He, *Macromolecules* **2011**, *44*, 3958.
[6] a) E. D. Laird, C. Y. Li, *Macromolecules* **2013**, *46*, 2877; b) L. Jia, A. Petretic, G. Molev, G. Guerin, I. Manners, M. A. Winnik, *ACS Nano* **2015**, *9*, 10673.
[7] a) R. C. Hayward, D. J. Pochan, *Macromolecules* **2010**, *43*, 3577; b) C. Chen, R. A. L. Wylie, D. Klinger, L. A. Connal, *Chem. Mater.* **2017**, *29*, 1918; c) Y. Mai, A. Eisenberg, *Chem. Soc. Rev.* **2012**, *41*, 5969; d) D. Klinger, M. J. Robb, J. M. Spruell, N. A. Lynd, C. J. Hawker, L. A. Connal, *Polym. Chem.* **2013**, *4*, 5038; e) J. Zhu, R. C. Hayward, *J. Am. Chem. Soc.* **2008**, *130*, 7496; f) H. Cui, Z. Chen, S. Zhong, K. L. Wooley, D. J. Pochan, *Science* **2007**, *317*, 647.
[8] a) A. H. Gröschel, T. I. Löbling, P. D. Petrov, M. Müllner, C. Kuttner, F. Wieberger, A. H. E. Müller, *Angew. Chem., Int. Ed.* **2013**, *52*, 3602; b) J. Zou, L. Liu, H. Chen, S. I. Khondaker, R. D. McCullough, Q. Huo, L. Zhai, *Adv. Mater.* **2008**, *20*, 2055; c) T. Gegenhuber, A. H. Gröschel, T. I. Löbling, M. Drechsler, S. Ehlert, S. Förster, H. Schmalz, *Macromolecules* **2015**, *48*, 1767; d) D. Fong, A. Adronov, *Chem. Sci.* **2017**, *8*, 7292.
[9] a) S. A. Jenekhe, X. L. Chen, *Science* **1999**, *283*, 372; b) J. F. Reuther, D. A. Siriwardane, R. Campos, B. M. Novak, *Macromolecules* **2015**, *48*, 6890; c) M. Lee, B.-K. Cho, W.-C. Zin, *Chem. Rev.* **2001**, *101*, 3869.
[10] a) C. Cai, J. Lin, Z. Zhuang, W. Zhu, *Adv. Polym. Sci.* **2013**, *259*, 159; b) C. Cai, Y. Li, J. Lin, L. Wang, S. Lin, X.-S. Wang, T. Jiang, *Angew. Chem., Int. Ed.* **2013**, *52*, 7732; c) C. Yang, L. Gao, J. Lin, L. Wang, C. Cai, Y. Wei, Z. Li, *Angew. Chem., Int. Ed.* **2017**, *56*, 5546; d) C. Cai, J. Lin, Y. Lu, Q. Zhang, L. Wang, *Chem. Soc. Rev.* **2016**, *45*, 5985.
[11] A. H. Korayem, M. R. Barati, G. P. Simon, T. Williams, X. L. Zhao, P. Stroeve, W. H. Duan, *Langmuir* **2014**, *30*, 10035.
[12] W. H. Duan, Q. Wang, F. Collins, *Chem. Sci.* **2011**, *2*, 1407.
[13] a) J. J. L. M. Cornelissen, M. Fischer, N. A. J. M. Sommerdijk, R. J. M. Nolte, *Science* **1998**, *280*, 1427; b) M. Liu, L. Zhang, T. Wang, *Chem. Rev.* **2015**, *115*, 7304; c) E. Yashima, N. Ousaka, D. Taura, K. Shimomura, T. Ikai, K. Maeda, *Chem. Rev.* **2016**, *116*, 13752.
[14] a) P. Deria, C. D. Von Bargen, J.-H. Olivier, A. S. Kumbhar, J. G. Saven, M. J. Therien, *J. Am. Chem. Soc.* **2013**, *135*, 16220; b) M. Zheng, A. Jagota, E. D. Semke, B. A. Diner, R. S. McLean, S. R. Lustig, R. E. Richardson, N. G. Tassi, *Nat. Mater.* **2003**, *2*, 338; c) X. Zhang, L. Meng, Q. Lu, *ACS Nano* **2009**, *3*, 3200.
[15] L. Zhang, A. Eisenberg, *Macromolecules* **1999**, *32*, 2239.
[16] a) C. Yang, Q. Li, C. Cai, J. Lin, *Langmuir* **2016**, *32*, 6917; b) Z. Zhuang, C. Cai, T. Jiang, J. Lin, C. Yang, *Polymer* **2014**, *55*, 602.
[17] J. Määttä, S. Vierros, M. Sammalkorpi, *J. Phys. Chem. B* **2015**, *119*, 4020.
[18] Z. Li, M. Tang, W. Bai, R. Bai, *Langmuir* **2017**, *33*, 6092.